

# Observational constraints on thawing quintessence models

Timothy G. Clemson and Andrew R. Liddle

*Astronomy Centre, University of Sussex, Brighton BN1 9QH, United Kingdom*

29 November 2021

## ABSTRACT

We use a dynamical systems approach to study thawing quintessence models, using a multi-parameter extension of the exponential potential which can approximate the form of typical thawing potentials. We impose observational constraints using a compilation of current data, and forecast the tightening of constraints expected from future dark energy surveys, as well as discussing the relation of our results to analytical constraints already in the literature.

**Key words:** cosmology: theory

## 1 INTRODUCTION

Thawing quintessence models, in the terminology of Caldwell & Linder (2005), are those in which at early times the dark energy has a much lower density than matter, but where the dark energy density begins to evolve once it becomes a significant fraction of the total (Steinhardt, Wang & Zlatev 1999; Huey & Lidsey 2001; Nunes & Copeland 2002). It is characterized by an equation of state which is initially  $w = -1$  to high accuracy, and which then ‘thaws’ to  $w > -1$  by the present. Provided the thawing process is sufficiently slow, these models are in agreement with current observational data.

At first sight the initial conditions for thawing quintessence appear very unnatural, as they require the same fine-tuning of a small initial density that one finds with the cosmological constant. This fine-tuning could presumably be explained using the same sort of anthropic string landscape argument often invoked for a pure cosmological constant (Bousso & Polchinski 2000; Susskind 2003). However the case of thawing quintessence may in fact be more appealing, because at least for very steep potentials one can argue that quantum fluctuations of the quintessence field acquired during early Universe inflation may drive the field to low energy densities (Malquarti & Liddle 2002). A complete cosmology from inflation through to the present may well lead to a significant probability of thawing quintessence behaviour, without imposing additional anthropic constraints.

In light of this, it is useful to characterize the types of thawing model allowed by present data, and indeed there have been several papers recently exploring aspects of thawing quintessence models, though these have largely ignored the issue of naturalness of initial conditions. Inflationary models can be characterized by the slow-roll approximation, but as this is not generally valid for quintessence (Bludman 2004; Capone, Rubano & Scudellaro 2006; Linder 2006; Cahn, de Putter & Linder 2008) some papers have sought an analogue to this approach for dark energy (Scherrer & Sen 2008; Dutta & Scherrer 2008). Another method, employed by Crittenden, Majerotto & Piazza (2007), involves smoothness requirements on the potential, while other work has

developed a classification of dark energy models by means of a calibration of their time variation (Linder 2006; Linder 2008; Cahn et al. 2008; de Putter & Linder 2008). Analytical bounds on thawing potentials have previously been derived by Caldwell & Linder (2005), Linder (2006) and Barger, Guarnaccia & Marfatia (2006), who also considered previous observational constraints. Expansions of the putative quintessence potential, either using the flow equations (Huterer & Peiris 2007) or directly (Sahlén, Liddle & Parkinson 2007) have been used to explore broad classes of models to contrast the thawing and non-thawing regimes.

In this paper we analyze thawing models from a somewhat different perspective. We look at a multi-parameter potential family  $V(\phi)$ , which includes the exponential potential as a special case, and which has enough freedom that the family can represent arbitrary values of  $V$ ,  $dV/d\phi$ , and  $d^2V/d\phi^2$  at the initial field value. Reminiscent of the slow-roll approximation to inflationary observables, which depend only on the potential and its first few derivatives, we aim to capture with this potential the full spectrum of thawing quintessence phenomenology. This is then confronted with present observational data, and the capabilities of future data assessed, before a consideration of the analytical constraints derived in previous analyses of thawing behaviour.

## 2 THAWING QUINTESSENCE

### 2.1 Quintessence dynamics

We assume a minimally-coupled scalar field  $\phi$  acts as quintessence. The pressure/density relation is  $w = p/\rho$  with

$$p = \frac{\dot{\phi}^2}{2} - V(\phi), \quad \rho = \frac{\dot{\phi}^2}{2} + V(\phi), \quad (1)$$

where dots denote derivatives with respect to time and  $V(\phi)$  is the field’s self-interaction potential. The variation in  $\phi$  obeys the Klein–Gordon equation

$$\ddot{\phi} + 3H\dot{\phi} + V' = 0, \quad (2)$$

where the prime indicates a derivative with respect to  $\phi$ . This shows that the field rolls down the slope of its potential  $V(\phi)$  and that its motion is damped by the Hubble parameter which, in units with  $8\pi G = 1$ , may be written

$$H = \frac{\dot{a}}{a} = \sqrt{\frac{\rho_t}{3}}, \quad (3)$$

where  $a$  is the scale factor of the Universe and  $\rho_t$  is the total density. We assume a flat matter-dominated Universe throughout.

The following dynamical systems approach, equations (4) through (10), was developed by Copeland, Liddle & Wands (1998), de la Macorra & Piccinelli (2000), Ng, Nunes & Rosati (2001), and Scherrer & Sen (2008). Equations (2) and (3) may be rewritten in terms of three new variables;  $x$ ,  $y$  and  $\lambda$ , defined as

$$x \equiv \frac{\dot{\phi}}{\sqrt{6}H}, \quad y \equiv \sqrt{\frac{V(\phi)}{3H^2}}, \quad \lambda \equiv -\frac{V'}{V}. \quad (4)$$

For a Universe containing only matter and a scalar field, the system may be written as (Ng et al. 2001)

$$\frac{dx}{dN} = -3x + \lambda\sqrt{\frac{3}{2}}y^2 + \frac{3}{2}x(1+x^2-y^2), \quad (5)$$

$$\frac{dy}{dN} = -\lambda\sqrt{\frac{3}{2}}xy + \frac{3}{2}y(1+x^2-y^2), \quad (6)$$

$$\frac{d\lambda}{dN} = -\sqrt{6}\lambda^2(\Gamma - 1)x, \quad (7)$$

where  $N$  is the logarithm of the scale factor,  $N \equiv \ln a$ , and  $\Gamma$  is defined as (Steinhardt et al. 1999)

$$\Gamma \equiv \frac{VV''}{(V')^2}. \quad (8)$$

For typical potentials, including the one we introduce below,  $\Gamma$  is a function of  $\lambda$  (though only expressible as such if  $\lambda(\phi)$  has an analytic inversion) and hence the system is an autonomous one (see e.g. Fang et al. 2008), though this property is not needed in our analysis.

In a Universe with flat geometry, the density parameter of the scalar field becomes

$$\Omega_\phi = x^2 + y^2, \quad (9)$$

and its effective equation of state is

$$\gamma \equiv 1 + w = \frac{2x^2}{x^2 + y^2}. \quad (10)$$

## 2.2 Generalized thawing potential

The initial value of the scalar field is assumed to be fixed at some early time in the matter-dominated era, and can be set to zero without any loss of generality, i.e.  $\phi_i = 0$ . Having made this choice, we can then explore a wide range of thawing models by taking the quintessence potential to be of the form

$$V(\phi) = V_i \exp(-c\phi)[1 + \alpha\phi], \quad (11)$$

where  $V_i$  is the initial value of the potential, and  $c$  and  $\alpha$  are parameters. This form is useful because of two properties. Firstly, it reduces to the well-known exponential potential in the case  $\alpha = 0$ ; this property motivates our choice in favour of a simple Taylor expansion around the origin, as often used in direct reconstruction of the quintessence potential (e.g. Sahlén, Liddle & Parkinson 2005). Secondly, in the vicinity of the origin it can approximate arbitrary potentials up to their second derivative. In the limit  $\alpha \rightarrow c$  it can

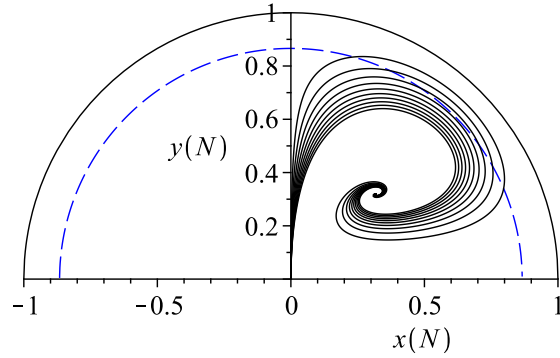


**Figure 1.** The evolution for  $\lambda_i = 0.1$  (outer curve) to 1 (inner curve) in steps of 0.1 for  $c = 4$ . The dashed semicircle represents the present-day dark energy density parameter  $\Omega_\phi \approx 0.75$ . Trajectories which reach this may correspond to the evolution of the Universe. The origin is the initial point at some early time during matter domination, and the unit semicircle represents domination by the scalar field.

also approximate the hilltop quintessence models recently studied by Dutta & Scherrer (2008).

Our results will therefore have two separate interpretations. The first is to consider equation (11) to be an exact potential (somewhat similar to the Albrecht–Skordis (2000) potential), valid for all  $\phi$ , enabling generalization of results from the exponential case. The second is to consider the results to be valid for *all* thawing potentials, provided the variation in  $\phi$  is small enough that our potential is a good local approximation to an arbitrary potential. We will take the convergence condition for this potential to be  $|\alpha\phi| \leq 0.1$ . We also restrict the parameters to  $c \geq \alpha$  so that initially  $V' \leq 0$  and hence the field value increases with time.

Putting this potential into equation (7) leads to

$$\frac{d\lambda}{dN} = \sqrt{6}(\lambda - c)^2x, \quad (12)$$

and the initial value of  $\lambda$  is given by

$$\lambda_i = c - \alpha. \quad (13)$$

We now allow the system to evolve out of an initial perturbation from  $\phi_i = 0$ , exploring the parameter space by plotting the evolution of the system over time for a range of values of  $\alpha$  and  $c$  (e.g. see Fig. 1). Equation (9) implies that  $0 \leq x^2 + y^2 \leq 1$  and so the resulting trajectories are confined to within the unit circle. From the definitions of  $x$  and  $y$ , equation (4), it can also be seen that making  $y$  negative and reversing the temporal coordinate (and thus  $\dot{\phi} \rightarrow -\dot{\phi}$ ), results in symmetrical behaviour below the axis to that above. Only the upper half-disc therefore need be considered for a full picture of possible trajectories. Furthermore, the lower half-disc corresponds to a contracting Universe, which is ruled out by observations as far as the past and present Universe is concerned.

Our initial condition keeps the initial scalar field velocity at zero, which is not quite appropriate. Cahn et al. (2008) carried out an analysis of the early-time behaviour of quintessence fields to compute the leading-order early-time behaviour of the velocity. In our case this translates as  $x_i \propto y_i^2$ , meaning that the initial velocity is indeed highly suppressed. We confirmed numerically that the difference to the trajectories is completely negligible.

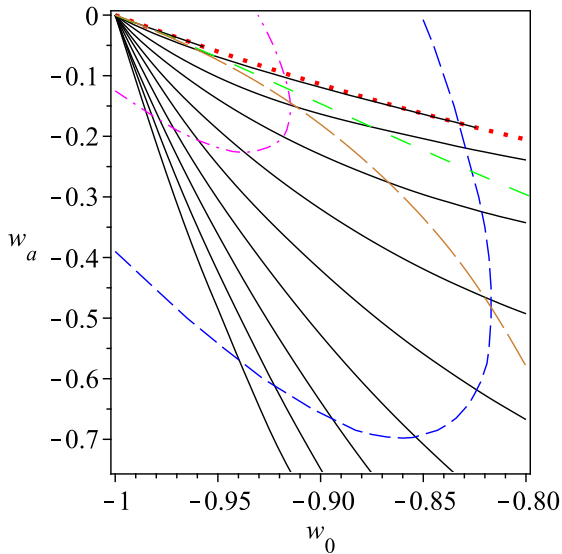


**Figure 2.** Families of potentials which reach  $\Omega_\phi = 0.75$ , and have positive values of the parameter  $\alpha$ , for  $c = 0.5$  (top solid line) to 5 (lowest solid line) in steps of 0.5. The short-close-dashed line delineates the range of values allowed by recent observational data and the dotted line represents the limit where  $\alpha = 0$ . The dot-dash line indicates the ten-year observational prospects discussed in Section 3.2, while the spaced-dashed and the long-dashed curves represent potentials with  $\Gamma_i = 0$  and  $\Gamma_0 = 0$  respectively.

### 3 OBSERVATIONAL CONSTRAINTS

#### 3.1 Current constraints

The present-day dark energy density parameter has an observed value of  $\Omega_\phi \approx 0.75$  (Komatsu et al. 2008) and using equation (9) we can determine which trajectories reach this value and as such may be representative of the real world (e.g. Fig. 1).

The set of possible models is better constrained, however, by considering their representation in the  $w_0$ - $w_a$  plane. Thawing dark energy is well parameterized by the equation (Chevallier & Polarski 2001; Linder 2003)

$$w(a) = w_0 + w_a(1 - a), \quad (14)$$

where  $w_0$  represents the present-day value of  $w$ , and  $w_a$  determines the change in  $w$  with the scale factor  $a$ . Equation (10) can now be used to derive expressions for  $w_0$  and  $w_a$  in terms of the variables of the autonomous system. Since  $a = 1$  at the present day we have

$$w_0 = \frac{x_0^2 - y_0^2}{x_0^2 + y_0^2}, \quad (15)$$

where  $x_0$  and  $y_0$  are the present-day values of  $x$  and  $y$ . The observational constraint that  $w$  is close to  $-1$  therefore requires viable trajectories to remain close to the  $y$ -axis at the time they reach the semicircle indicating the correct dark energy density.

The time dependence of the equation of state is also observationally constrained, though less strongly. Combining equations (10) and (14) leads to the expression for  $w_a$

$$w_a = -\frac{4x_0y_0}{(x_0^2 + y_0^2)^2} \left( -3x_0y_0 + \lambda_0 \sqrt{\frac{3}{2}} y_0^3 + \lambda_0 \sqrt{\frac{3}{2}} x_0^2 y_0 \right), \quad (16)$$

where  $\lambda_0$  is the present-day value of  $\lambda$ .

The coordinates at which trajectories reach the present dark energy density can now be used in these two equations to plot the

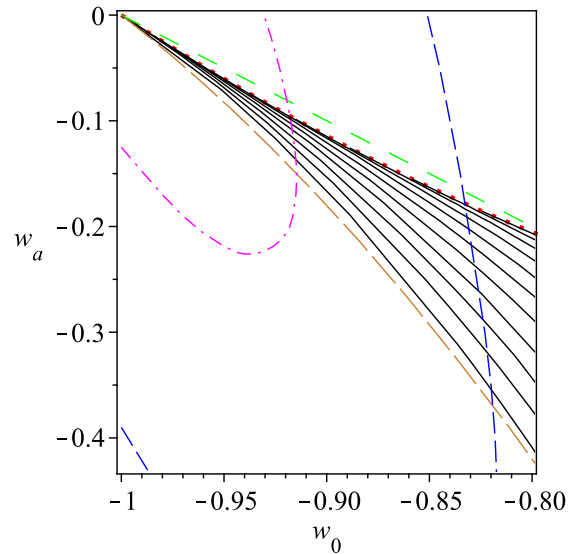


**Figure 3.** As Fig. 2, but for potentials with negative values of the parameter  $\alpha$  and  $c = 0$  (lowest solid curve) to 1 (top solid line) in steps of 0.1. The spaced-dashed line is the  $-w_a \geq 1 + w_0$  thawing limit, while the long-dashed curve represents the curve where  $X = 3/4$  (see Section 4).

predictions from families of potentials in the  $w_0$ - $w_a$  plane, shown in Figs. 2 and 3. These values are compared to the observationally-allowed region (short-close-dashed curve) obtained by Komatsu et al. (2008) from a combination of baryon acoustic oscillation, type 1A supernovae and WMAP5 data at a 95% confidence limit, and would only be marginally improved by the inclusion of big-bang nucleosynthesis constraints.

One might further worry whether the approximation of constant  $w_a$  is accurate enough, and indeed Dutta & Scherrer (2008) indicated that in some parameter regions it will not be. We quantify this below by delineating the regions of parameter space in which  $w_a$  has varied by more than 25% from redshift one to the present.

Each of the solid curves in Figs. 2 and 3 represents a family of potentials with the same value of the parameter  $c$  in the exponent, but different values of the linear parameter  $\alpha$  and therefore  $\lambda_i$  (remember  $\lambda_i = c - \alpha$ ). They are *not* the evolutionary tracks of particular potentials, but rather indicate the points in the  $w_0$ - $w_a$  plane which different potentials have reached at the present day. The largest values of  $\alpha$  are at the left-hand end of the curves in Fig. 2, where they all share a common origin at the point  $[-1, 0]$ , corresponding to the cosmological constant. Potentials at this point have  $c = \alpha$  which means that  $\lambda_i = 0$  and so they are flat, while nearby potentials have negative curvature, ie.  $\Gamma < 0$ , and correspond to the case of hilltop quintessence as described by Dutta & Scherrer (2008). Moving to the right along the curves the potentials have decreasing values of  $\alpha$  and hence increasing  $\lambda_i$ , ie. increasingly negative initial slope.

Useful orientation into the behaviour of the family of models comes from studying the time dependence of  $\Gamma$ . We see from equation (12) that  $\lambda$  is monotonically increasing with time, and hence  $\Gamma$  too is an increasing function whose initial value may be positive or negative (we keep  $c > 0$  throughout, corresponding to  $\phi$  increasing with time). The sign of  $\Gamma$  is the same as of  $V''$ , and hence determines whether the potential is steepening or become more shallow with time, with  $\Gamma = 0$  corresponding to a point of inflection in the potential. We can then classify the models as follows. If the ini-

tial value of  $\Gamma$ ,  $\Gamma_i$ , is already positive, then  $\Gamma$  stays positive forever and the potential is becoming shallower with time (the exponential case is the archetypal example). If the *present* value of  $\Gamma$ ,  $\Gamma_0$ , is negative, then  $\Gamma$  has been negative throughout the past evolution of the Universe, corresponding to a steepening potential as in hilltop quintessence. If neither of these conditions is satisfied, then  $\Gamma$  changes from negative to positive during the evolution, with the potential initially steepening and later becoming more shallow.

In the figures, the curvature of the potentials increases to the right and eventually potentials with  $\Gamma_0 = 0$  (long-dashed) and subsequently  $\Gamma_i = 0$  (spaced-dashed line) are reached, corresponding to points of inflection in the potential curve. After the points of inflection the slope of the potentials increases along the curves, which then all head towards the exponential limit as  $\alpha$  approaches zero. They eventually graze the exponential curve where  $c = \lambda = \text{constant}$  and the curvature reaches its maximum value of  $\Gamma_i = 1$ . Higher values of  $c$  than those plotted in Fig. 2 are possible, but only as long as  $c \approx \alpha$ . For example, the trajectory of  $c = 20$  in the  $x$ - $y$  plane only reaches the dark energy density parameter curve when  $c - \alpha \leq 10^{-10}$ .

The curves in Fig. 3 represent similar families of potentials to those in Fig. 2 but with negative values of the parameter  $\alpha$ . These curves begin from the exponential limit at their left-hand end and have increasingly negative values of  $\alpha$  to the right. This means that they have increasing  $\lambda_i$ , i.e. the initial slope of the potentials becomes ever steeper to the right. Here the curves once again diverge from the exponential case as the magnitude of  $\alpha$  increases. This is a consequence of their increasing linearity, which causes the curves to asymptotically approach the family of linear potentials with  $c = \Gamma = 0$ , as eventually  $\lambda_i \approx c$ . Eventually each family of curves comes into conflict with observations, which therefore give a lower limit on  $\alpha$  for each value of  $c$ . The region of potentials in the  $c$ - $\alpha$  parameter space consistent with the observational constraints is shown in Fig. 4.

The range of potentials for which convergence remains good up until the present day can be found by rewriting the convergence condition as

$$0.9 < \frac{\alpha}{c - \lambda_0} < 1.1, \quad (17)$$

and is also shown in Fig. 4. Potentials with  $c < 0$  are not considered here, since they simply correspond to those for which the field rolls in the opposite direction and so add nothing new to the analysis. Figure 4 also shows the region (essentially  $\alpha \geq 1$ ) where the assumption of constant  $w_a$  used in our observational comparison is breaking down; the observational results should be considered less robust in this region.

Admitting potentials with  $\alpha < 0$  allows  $V(\phi)$  to become negative in the future, which may prompt future recollapse of the Universe (Kallosh et al. 2003). Such potentials are included in our analysis, though they may be considered as being approximate representations of the behaviour of arbitrary potentials from early times to the present day, without necessarily extrapolating into the negative energy density regime.

The representation of our results in terms of the more familiar slow-roll parameters from inflation,  $\epsilon$  and  $\eta$ , is easily found from their definitions (in natural units)

$$\epsilon_i \equiv \frac{1}{2} \left( \frac{V'_i}{V_i} \right)^2 = \frac{1}{2} \lambda_i^2, \quad (18)$$

$$\eta_i \equiv \frac{V''_i}{V_i} = 2c\lambda_i - c^2, \quad (19)$$

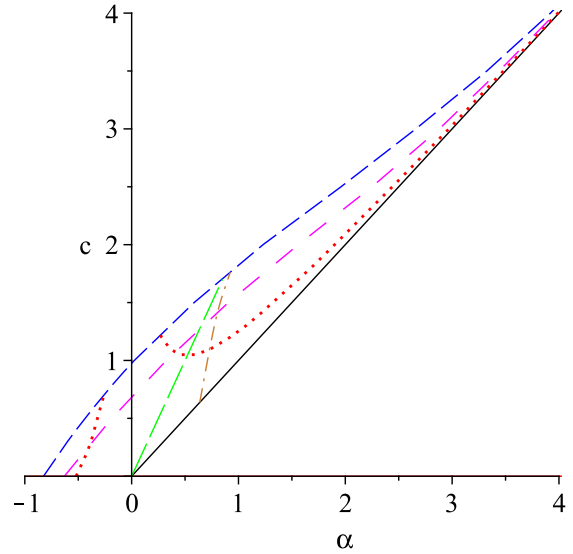


**Figure 4.** The allowed potentials in the  $c$ - $\alpha$  parameter space. The region beneath the short-dashed line is allowed by the observational constraints, while the spaced-dash line below it gives an approximation to the ten-year observational prospects discussed in Section 3.2. The region between the dotted lines contains potentials for which convergence remains good ( $|\alpha\phi| < 0.1$ ) up until the present day and the solid line represents the physical limit for which  $\lambda$  is positive (i.e.  $dV/d\phi$  remains negative). Models to the left of the dot-dashed line have  $w_a$  constant to a good approximation; our observational treatment is less reliable for those to the right of this line. Finally, the long-dashed line is where  $\Gamma_i = 0$ , which divides the parameter space into shallowing potentials on the left and those which undergo a period of steepening on the right.

and is shown in Fig. 5. As would be expected from the results of Scherrer & Sen (2008) and Dutta & Scherrer (2008), the assumption of constant  $w_a$  fails for large negative  $\eta$  (the top panel), meaning our observational comparison method is not robust, but is fine otherwise.

### 3.2 Future prospects

As well as the present-day observational constraints, we can use predictions of future bounds to give a sense of how the range of possible potentials may be further restricted. Each graph (except Fig. 6) displays an approximation to the ten-year observational prospects (dot-dashed curve) under the assumption that  $\Lambda$ CDM is the true model. This was achieved by approximating the predicted future  $w_0$ - $w_a$  limits from the literature and then resizing the present observational constraints to fit them, thereby assuming similarly distributed future constraints. These constraints roughly correspond to predictions for both forthcoming Stage 3 programmes, such as the Dark Energy Survey, at 68% c.l. (Abbott et al. 2005) and future Stage 4 projects, such as JDEM, at 95% c.l. (Albrecht et al. 2006). Figs. 2 and 3 show that a significant limiting of the allowed region in the  $w_0$ - $w_a$  plane is possible over the next ten years, but Fig. 4 shows that this does not translate into a correspondingly large reduction in the  $c$ - $\alpha$  parameter space used in our model. There is however a slightly greater reduction in the size of the allowed region in the  $\eta$ - $\epsilon$  plane, as shown in Fig. 5.

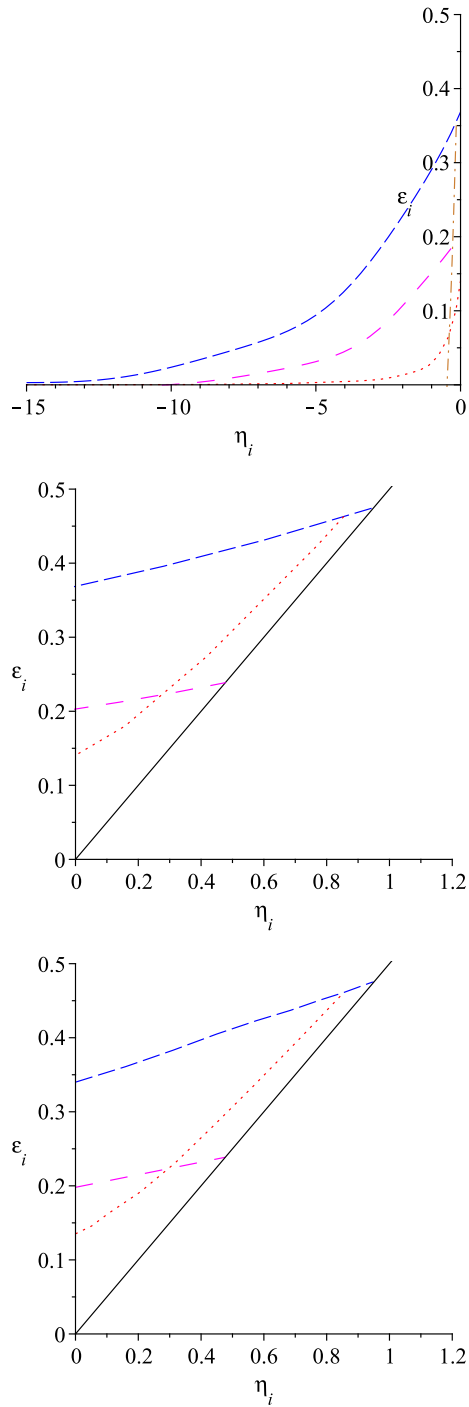


**Figure 5.** The allowed region of potentials in the  $\eta$ - $\epsilon$  plane. Positive  $\alpha$  with negative  $\Gamma_i$  is shown on at the top, positive  $\alpha$  with positive  $\Gamma_i$  is shown in the middle, and negative  $\alpha$  (all of which have  $\Gamma_i > 0$ ) are at the bottom. The lower two figures correspond to potentials which have been shallowing throughout their history. The region below the dashed line is consistent with present observations and the space-dash line gives an approximation to the ten-year observational prospects discussed in Section 3.2. Potentials below the dotted line all have  $|\alpha\dot{\phi}| < 0.1$  up until the present day, and so converge well. The  $\epsilon$  axis is where  $\Gamma_i = 0$  and the  $\eta$  axis is where  $\alpha = c$ , while the solid line in the lower two figures represents the limit where  $\alpha = 0$ . In the top figure, only models to the right of the dot-dash line have  $w_a$  constant to a good approximation (this condition is always satisfied in the lower two graphs).

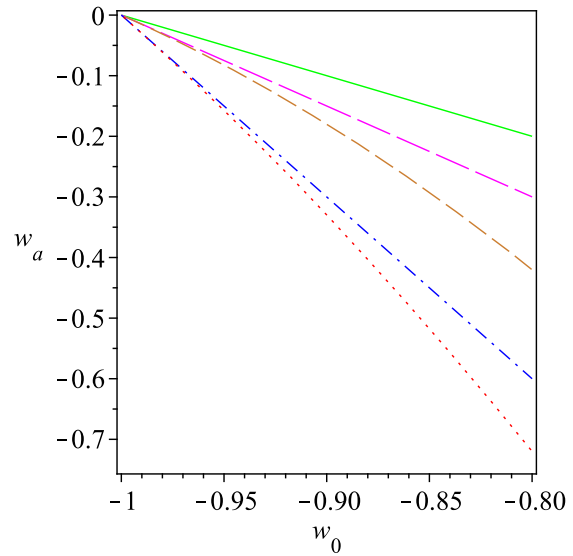


**Figure 6.** The solid line is the upper thawing bound of  $-w_a \geq 1 + w_0$ , the long-dashed line is the Barger et al. (2006) limit and the short-dashed curve is where  $X = 3/4$ . The dot-dashed line is the original Caldwell & Linder (2005) lower thawing bound and the dotted line is the curve where  $X = 3/2$ .

#### 4 ANALYTICAL CONSTRAINTS

A number of different analytical constraints have been placed on thawing models and the present situation could perhaps bear some clarification. Fig. 6 shows constraints in the  $w_0$ - $w_a$  plane from previous analyses of thawing dynamics. The upper limit holds in all cases, as only below this line is the requirement  $w > -1$  fulfilled, ie.  $-w_a \geq 1 + w_0$  (solid line). Also, from the original definition of thawing behaviour by Caldwell & Linder (2005), comes the lowest of the linear boundaries,  $-w_a \leq 3(1 + w_0)$  (dot-dashed line). This comes from the requirement that  $\ddot{\phi}t < \dot{\phi}$  for potentials where  $\dot{\phi}$  is decreasing for all time. The slope of such potentials is monotonically increasing (becoming less negative) as the field asymptotically approaches the minimum of its potential curve.

Linder (2006) defined two useful ratios of the Klein-Gordon terms and the relationship between them

$$X \equiv \frac{\ddot{\phi}}{H\dot{\phi}}; \quad Y \equiv \frac{\ddot{\phi}}{V'}; \quad X = -3\frac{Y}{1+Y}. \quad (20)$$

The Klein-Gordon equation can be used along with these definitions to obtain an expression for  $X$  in terms of  $x$ ,  $y$  and  $\lambda$

$$X = 3 \left( \frac{\lambda y^2}{\sqrt{6}x} - 1 \right). \quad (21)$$

This allows us to plot given values of  $X$  using the generalized potential. The aforementioned lower bound of  $-w_a \leq 3(1 + w_0)$  was shown by Linder (2006) to be an approximation to the more precise limit of  $X = 3/2$  (dotted curve), although this curve does still contain the implicit approximation that  $H \approx 2/3t$ . Barger et al. (2006) applied the original Caldwell & Linder (2005) bound at a redshift of 1, allowing for a significant tightening of the constraints on potentials with monotonically increasing slope and showed that such potentials satisfy  $-w_a > (3/2)(1 + w_0)$  (long-dashed line). This is again a linear approximation and we plot this bound as the more accurate curve where  $X = 3/4$  (short-dashed curve).

Potentials which steepen as the field rolls down may still sat-

isfy the basic requirement for thawing that  $w$  begins very close to  $-1$  before increasing at later times, despite permitting a more complex thawing behaviour. In principle their range extends all the way to the  $w_0 = -1$  line, which represents the divide from the present-day phantom regime but, as mentioned in Section 3.1, in our model such potentials need to be increasingly finely tuned the closer they are to  $w_0 = -1$ . Linder (2006) mentioned that potentials which steepen as the field rolls down should lie below the bound of  $\dot{\phi}t < \phi$ . We find that this requirement however, whilst sufficient to ensure that potentials steepen as the field rolls down, is not a *necessary* condition. We find that potentials which do undergo a period of steepening slope since the onset of matter domination all lie beneath the curve where  $\Gamma_i = 0$  (spaced-dashed line) in Fig. 2. This represents the limit below which the potentials have all reached the point of inflection in the generalized potential curve by the initial early time during matter domination. We find that this *coincidentally* corresponds to a very good accuracy to the aforementioned Barger et al. (2006) linear bound, which may therefore be used as an upper limit for potentials which have not had monotonically-increasing slope throughout matter domination.

The long-dashed curve in Fig. 2 shows potentials for which  $\Gamma_0 = 0$ , ie. they reach their point of inflection at the present day, and as such have been steepening throughout matter domination. Potentials between this curve and the  $\Gamma_i = 0$  line are therefore those which have crossed their point of inflection at some time during the matter-dominated epoch, and so the distance between these two curves is related to the age of the Universe. It should also be noted that above the  $X = 3/4$  curve (long-dashed in Fig. 3) there are always two potentials at each point in the  $w_0-w_a$  plane, and above the  $\Gamma_i = 0$  curve (spaced-dashed in Fig. 2) there are always two potentials with monotonically increasing slope at each point.

Potentials above the  $\Gamma_i = 0$  curve in Fig. 2 and those with negative  $\alpha$  (ie. all those in Fig. 3), have all had positive curvature ( $\Gamma_i > 0$ ), and as such increasingly shallower slope, since the initial time. These are the potentials to which the Caldwell & Linder (2005), Linder (2006), and Barger et al. (2006) limits all apply. We find that the lower limit on such potentials is the case where  $c = 0$ , i.e. the family of linear potentials. Since linear potentials lie approximately along the curve of  $X = 3/4$  we find that this could therefore be used as a lower bound on potentials with monotonically increasing slope to which the previous limits have been applied, as shown in Fig. 3 (long-dashed curve). Also shown in Fig. 3 is our finding that the exponential potentials (large-dotted curve) represent an upper limit and may still be best approximated by the original Caldwell & Linder (2005) upper bound (spaced-dashed line).

## 5 CONCLUSIONS

The form of the scalar field self-interaction potential studied here allows observational constraints to be placed on thawing quintessence models, encompassing a wide range of thawing behaviour. A pure exponential potential for example, which has the greatest observationally-allowed slope ( $\lambda_i \approx 1$ ), is currently restricted to having  $c$  less than about 1, and upcoming observations could reduce this by up to a third. Despite applying strict convergence conditions, we expect the chosen potential to be fairly reliable within the whole of the observationally-allowed region. This is especially true when considering the ten-year observational prospects, for which the value of  $|\alpha\phi|$  peaks at around 0.3.

The analytical constraints on thawing models in the  $w_0-w_a$

plane are tightest for potentials which have had monotonically increasing slope throughout their evolution history. Their range may be reasonably well approximated using limits from previous analyses, but within these bounds there are always two potentials at any given point in the  $w_0-w_a$  plane. Potentials which have undergone a period of decreasing slope have an upper bound which is lower than that for purely shallowing potentials, and which is coincidentally well approximated by an existing limit, but only fine-tuning arguments restrict these potentials otherwise. Future data will require new analytical constraints to be fitted to potentials in the thawing region for the sake of accuracy, but for now existing limits properly applied offer a fairly accurate representation of the true range of viable models.

## ACKNOWLEDGMENTS

T.G.C. was supported by the Royal Astronomical Society and A.R.L. by STFC. We thank the referee, Bob Scherrer, for raising important points in his report.

## REFERENCES

- Abbott T. et al., 2005, arXiv:astro-ph/0510346  
 Albrecht A. et al., 2006, arXiv:astro-ph/0609591  
 Albrecht A., Skordis C., 2000, Phys. Rev. Lett., 84, 2076  
 Barger V., Guarnaccia E., Marfatia D., 2006, Phys. Lett., B635, 61  
 Bludman S., 2004, Phys. Rev. D, 69, 122002  
 Bousoo R., Polchinski J., 2000, JHEP, 06, 006  
 Cahn R. N., de Putter R., Linder E. V., 2008, JCAP, 0811, 015  
 Caldwell R. R., Linder E. V., 2005, Phys. Rev. Lett., 95, 141301  
 Capone M., Rubano C., Scudellaro P., 2006, Europhys. Lett., 73, 149  
 Chevallier M., Polarski D., 2001, Int. J. Mod. Phys., D10, 213  
 Copeland E. J., Liddle A. R., Wands D., 1998, Phys. Rev. D, 57, 4686  
 Crittenden R., Majerotto E., Piazza F., 2007, Phys. Rev. Lett., 98, 251301  
 de la Macorra A., Piccinelli G., 2000, Phys. Rev., D61, 123503  
 de Putter R., Linder E. V., 2008, JCAP, 0810, 042  
 Dutta S., Scherrer R. J., 2008, Phys. Rev. D, 78, 123525  
 Fang W., Li Y., Zhang K., Lu H.-Q., 2008, arXiv:0810.4193  
 Huterer D., Peiris H. V., 2007, Phys. Rev. D, 75, 083503  
 Huey G., Lidsey J. E., 2001, Phys. Lett., B514, 217  
 Kallosh R., Kratochvil J., Linde A., Linder E. V., Shmakova M., 2003, JCAP, 0310, 015  
 Komatsu E. et al., 2008, arXiv:0803.0547  
 Linder E. V., 2003, Phys. Rev. Lett., 90, 091301  
 Linder E. V., 2006, Phys. Rev. D, 73, 063010  
 Linder E. V., 2008, Gen. Rel. Grav., 40, 329  
 Malquarti M., Liddle A. R., 2002, Phys. Rev. D, 66, 023524  
 Ng S. C. C., Nunes N. J., Rosati F., 2001, Phys. Rev. D, 64, 083510  
 Nunes N. J., Copeland E. J., 2002, Phys. Rev. D, 66, 043524  
 Sahlén M., Liddle A. R., Parkinson D., 2005, Phys. Rev. D, 75, 023502  
 Sahlén M., Liddle A. R., Parkinson D., 2005, Phys. Rev. D, 72, 083511  
 Scherrer R. J., Sen A. A., 2008, Phys. Rev. D, 77, 083515  
 Steinhardt P. J., Wang L., Zlatev I., 1999, Phys. Rev. D, 59, 123504  
 Susskind L., 2003, arXiv:hep-th/0302219

This paper has been typeset from a  $\text{\TeX}/\text{\LaTeX}$  file prepared by the author.